Rev. Adv. Mater. Sci. 50 (2017) 1-12

GRAPHENE-MODIFIED BULK NICKEL COMPOSITE - INVESTIGATION OF STRUCTURE AND MECHANICAL CHARACTERISTICS

V.G. Konakov[1,2], O.Yu. Kurapova[1,2], I.V. Lomakin[1,2], N.N. Novik[1,2], S.N. Sergeev[3], E.N. Solovyeva[4], A.P. Zhilyaev[3], I.Yu. Archakov[1,5] and I.A. Ovid'ko

[1]Peter the Great St. Petersburg Polytechnic University, St.Petersburg 195251, Russia
[2]St. Petersburg State University, St. Petersburg, 199034 Russia
[3]Institute of Metals Superplasticity Problems, Russian Academy of Sciences, Ufa, 450001, Russia
[4]Glass and Ceramics Ltd., St. Petersburg, 199004, Russia
[5]Institute for Problems of Mechanical Engineering, Russian Academy of Sciences, St. Petersburg, 199178, Russia

Received: October 20, 2016; revised: July 14, 2017

Abstract. The present work reports the detailed investigation of graphene-modified bulk nickel composites with graphene+graphite phase content up to 4.7 at.%. The composites were fabricated using ball milling and powder metallurgy methods with nickel nanopowder and exfoliated graphite being starting materials. Phase composition and composites structure were studied via X-ray diffraction technique (XRD), Differential scanning calorimetry (DSC), Raman spectroscopy (RS) and scanning electron microscopy (SEM). The effect of graphene addition on the grains size and orientation was determined from backscattered electrons images (EBSD technique). The effect of graphene-graphite phase content on the mechanical properties of the composite was studied. It was shown that small amounts of this phase result in the graphene formation on the surface of metal grains; in turn, this phenomenon affects the composite mechanical properties: its hardness increases, its plasticity decreases, and the strength value remains on the same level. The increase in the graphene-graphite phase content results in graphene flakes formation and new phase allocation corresponding to graphite, leading to the plasticity recovery and in the significant decrease of hardness and strength.

1.INTRODUCTION

Graphene (Gr) is a two-dimentional material, formed by sp^2 hybridized carbon atoms. Since its discovery by Geim and Novoselov in 2004 [1,2], it has attracted considerable attention because of the unique mechanical, chemical and electrophysical properties. Chemical stability, high thermal and electrical conductivity, exceptional conductivity, exceptional mechanical characteristics, optical transparency, and high surface area of graphene make it possible to use it for novel materials fabrication in the field of energy conversion [3], supercapacitors [4], gaseous sensors [5,6], field electric transistors (FETs) [7], etc. The outstanding mechanical characteristics of graphene should be also mentioned. In particular, the yield stress of Gr according to molecular dynamics simulations is 0.912 TPa [8], Young's modulus and tensile strength of graphene monolayer being 1.1 TPa and 130 GPa, respectively [9]. The decrease of mechanical properties with the increase of layers in the graphene flake makes it

Corresponding author: V. G. Konakov, e-mail: glasscer@yandex.ru

perfect reinforcement addition for composite materials fabrication [10]. It was shown that ”polymer matrix – graphene” composites exhibit higher mechanical strength and enhanced electrical conductivity comparing to “polymer matrix – graphite” and polymer matrix – carbon nanotubes” composites (polymer matrix - CNTs [11-13]. Moreover, Gr found a wide application as an additive for metallic matrices reinforcement [14]. The incorporation of small graphene addition to Al leads to Vickers hardness and tensile strength values increase (up to 62 %) in the composites [15,16]. Similar effects of graphene addition were reported for magnesium [17] and copper [18] composites.

Metal matrix nickel based composites find their application in automobile and aerospace industries as well as in turbine construction [19-22] due to high strength and sustainable fatigue combined with moderate plasticity and lower thermal expansion coefficients of Ni as compared to other constructing metals, e.g. Cu and Al. Ceramic powders, i.e. SiC, Al_2O_3, and WC [23-25], as well as different types of CNTs are the most commonly used additions to metals [26]. In contrast to CNT's, graphene can be distributed homogeneously in the nickel matrix, which allows enhancement of the mechanical properties of nickel composites. So far, there are few works devoted to the fabrication of graphene, reduced graphene oxide (rGO), and graphene oxide (GO) doped nickel composites. The outstanding work of Zhao et al. [27] describing “nickel-rGO composite” manufacturibg via molecular mixing technique and spark plasma sintering should be mentioned here. In this work, it was shown that the addition of Gr favors the applied load redistribution and effectively blocks the dislocation growth. The extreme character of mechanical characteristics dependence on rGO concentration was also shown with the maximal values being at ~1.5 wt.% rGO.

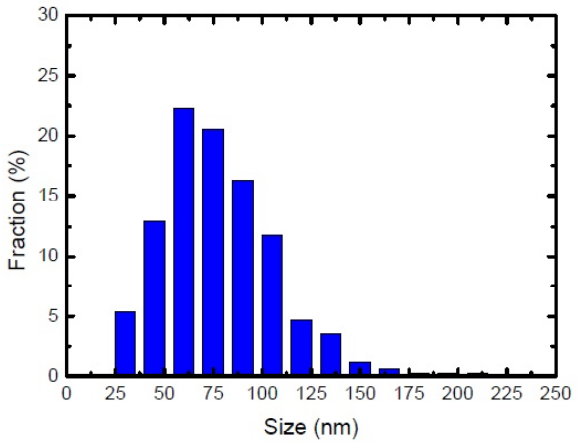

Fig. 1. Particle size distribution in starting nanoNi powder.

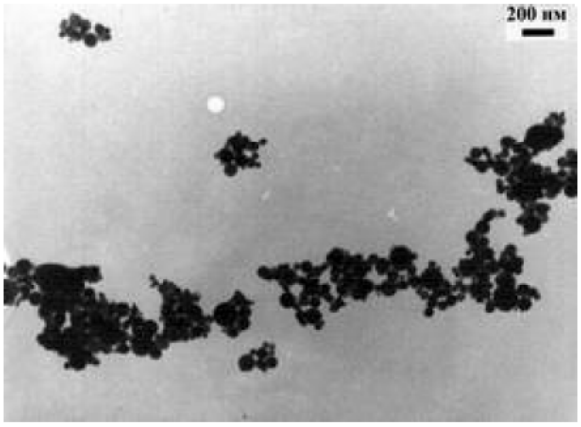

Fig. 2. Typical microphotograph of nanoNi powder.

Powder metallurgy technique, i.e. the mixing of powders of metal and dopant with their further sintering, is one of the simple and effective ways to manufacture “metal matrix-carbon composites”. In case of copper [28,29], aluminium [30], and tungsten [31] matrix composites with the addition of ceramics powders and CNTs, particle size distribution in the starting powders affects the homogeneity of composite components distribution and the structure of the reinforcing addition. It was shown that the decrease of the particle size of the starting powders leads to hardness and compressive strength increase. Great results have been recently obtained by authors in a field of bulk nickel-based composites [32]. Namely, in the fabrication procedure of metal-Gr composites, nickelnanopowder was for the first time in science successfully used for bulk nickel-based composite manufacturing. The use of nanopowders allowed the elimination of graphene agglomeration due to the high contact surface of matrix components and Gr. Thus, the present work is devoted to the fhe detailed characterization of the structure, phase composition and mechanical properties of novel nickel graphene-modified composites, obtained from nickel nanopowders. Special attention was paid to the allotropic form of carbon in the obtained materials.

2. EXPERIMENTAL

2.1. Sample preparation

Pure nickel, Ni - 0.47 at.% (Gr+graphite) and Ni – 4.7 at.% (Gr+graphite) composites were fabricated utilizing ball milling and powder metallurgy meth-

ods. The starting materials were commercial Ni nanopowder (Ni content ~99.7 wt.%; mean particle sizes of 70-80 nm; "Advanced Powder Technologies", Russia) and commercial exfoliated graphite platelets. Characterization of the powder particle size distribution is shown in Fig. 1, as seen from the figure, the fraction of particles with the size over 125 nm is less than 5%.

Fig. 2 presents typical microphotograph of the powder obtained using optical microscopy. Confirming the data on the particle average size, this image also demonstrates the evident tendency to particle agglomeration: a number of agglomerates with the average size of ~200-300 nm consisting of individual particles can be seen here. Note that such effect is typical for most metal nanopowders.

The mixture of starting powders specified by 0.47 and 4.7 at.% graphite contents were ball-milled for 2 h with 2 min reverse cycles at 400 rpm in a planetary mill Pulverisette-6. Following Refs. [33,34], this treatment effectively induces graphite-to-Gr transformations resulting in few-layer Gr nanoplatelets homogeneously mixed with metal nanoparticles. Also, pure Ni nanopowder was treated in the same way. Since Ni nanopowder is a highly flammable substance, all above operations were performed in a box with dry nitrogen atmosphere.

The milled (pure and mixed) nanosized powders were compacted for 15 min at the pressure of 12-12.5 t/cm^2 in stainless steel press forms. As a result, tablet-like specimens having 25 mm in diameter and 9 mm in height were fabricated.

The final synthesis step was the annealing in a vacuum furnace at 1523K. In this case, the temperature increase rate was 10 K/min, the exposure at maximum temperature was 1 h, and the cooling regime was "cooling with the furnace" (~ 6 h down

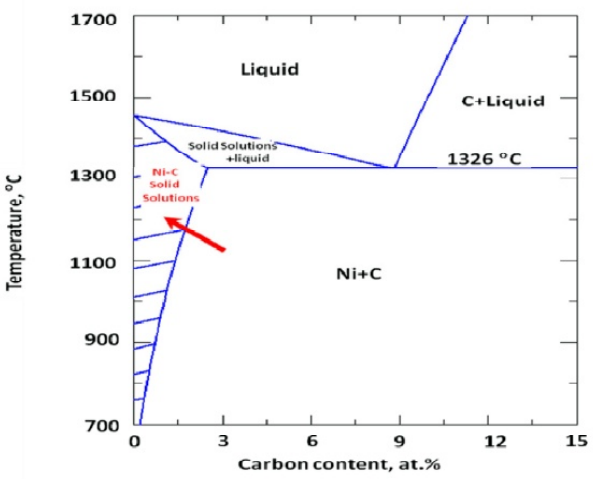

Fig. 3. Ni-C phase diagram, modified from [36].

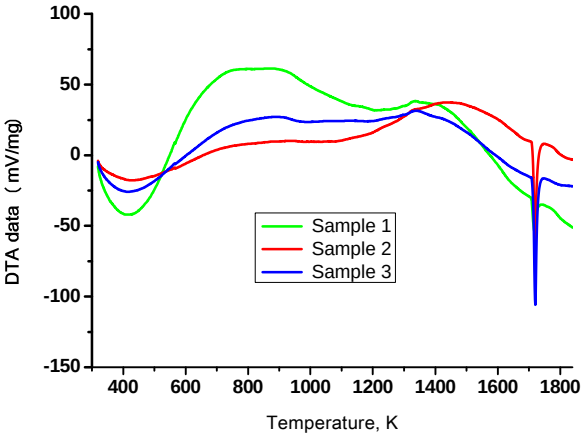

Fig. 4. DTA results for specimens studied.

to 773K). Hereinafter, the final specimens fabricated from pure Ni powder, mixed Ni - 0.47 at.% graphite and Ni – 4.7 at.% graphite powders will be called specimens 1, 2, and 3, respectively.

2.2. Specimens characterization

Possible chemical interactions and phase transitions in starting powders were considered from the results of synchronic thermal analysis (STA, NETZSCH STA 449 F3) in the temperature range 303-1773K in Ar ambiance, heating rate was 10K per minute. Phase composition of the initial powders and final specimens was identified by XRD (SHIMADZU XRD-6000, Cu-K_α, λ = 1.54 Å). Corresponding allotropic form of the carbon in the specimens was identified via Raman Spectroscopy (SENTERRA T64000, exciting radiation wave length 488 nm, gate voltage – 40 V).

Specimen microstructure was analyzed by SEM (Supra 55VP, accelerating voltage 20 keV) with the energy-dispersive X-ray spectroscopy (EDX) device for identification of chemical composition. In addition, EBSD study was performed (electronic microscope TESCANMIRA 3LMHFEG with EBSD device "CHANNEL 5", see [35] for the technique details). The obtained results were subjected to standard data processing. The accuracy of the misorientation angle determination was 2°, the accuracy of axis disorientation determination was 5°, and minimal grain size to determine was 3 pixels. Grain boundaries were determined as linear section between high-angle (HAB) grain boundaries with the misorientation higher 15°.

Vickers hardness was determined at the load of 3 N during 15 seconds (Micromet–5101, diamond, pyramid shaped indentor). The mechanical properties of the specimens 1, 2 and 3 in compression

Table 1. Characterization of phase transition from DTA results.

	SAMPLE		
	1	2	3
Melting temperature, K	1418	1420	1421
Enthalpy of fusion, ΔH, kcal/mol	0.382	1.171	1.434

tests (SHIMADZU AG X-Plus) were examined at 50 kN load with strain rate of 5×10^{-4} s^{-1}. The stress-strain dependences were plotted (each curve is averaged over 5 tests).

3. RESULTS AND DISCUSSION

Visual inspection of annealed specimens shows no changes in samples 1 and 2 after the heat treatment, while partial cracking was observed in specimen 3: the crack was observed in the plane parallel to tablet base at the height ~ ½ of the its height. It should be also noted that specimen 3 melted a bit on the corners upon annealing.

3.1. Phase composition of starting powders and specimens

Fig. 3 depicts the phase diagram calculated in [36] regarding for experimental data reported in [37]. As follows from the diagram, Ni-C solid solution formation is possible at carbon content up to 3 wt.%.

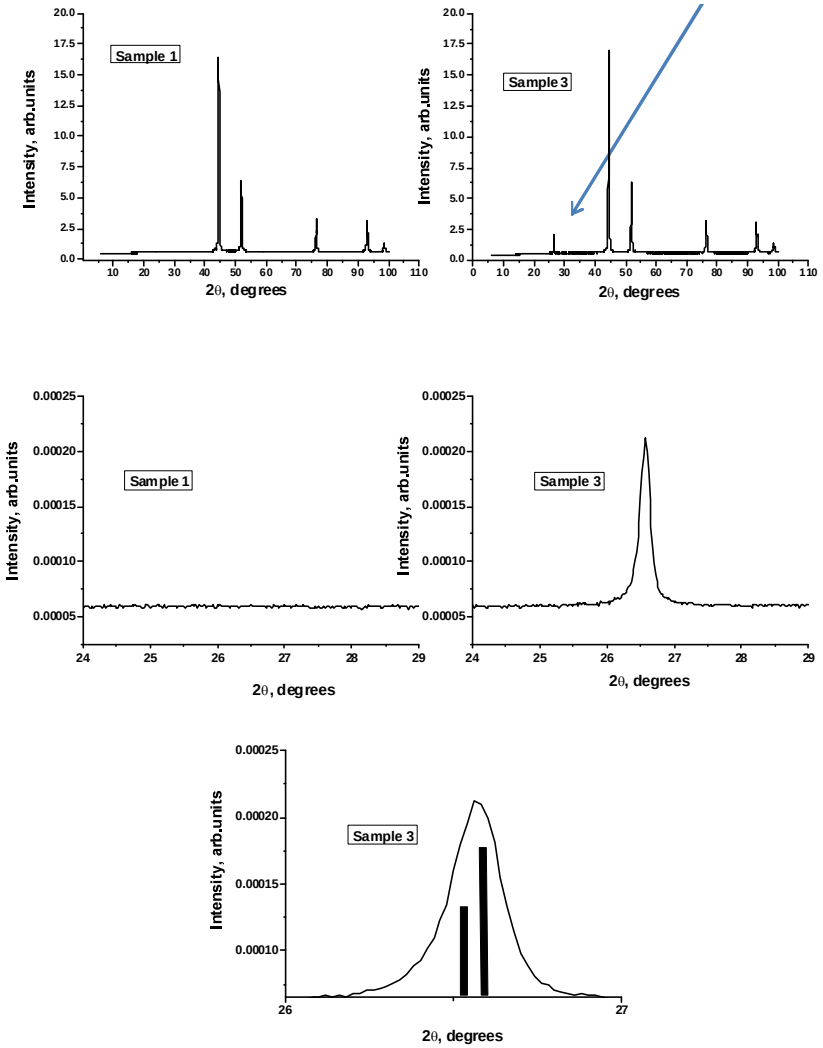

Fig. 5. Comparison of XRD patterns obtained for Specimens 2 and 3: upper row - general data; middle - magnified carbon peak region and the detalization of this reflex as a two peaks superposition.

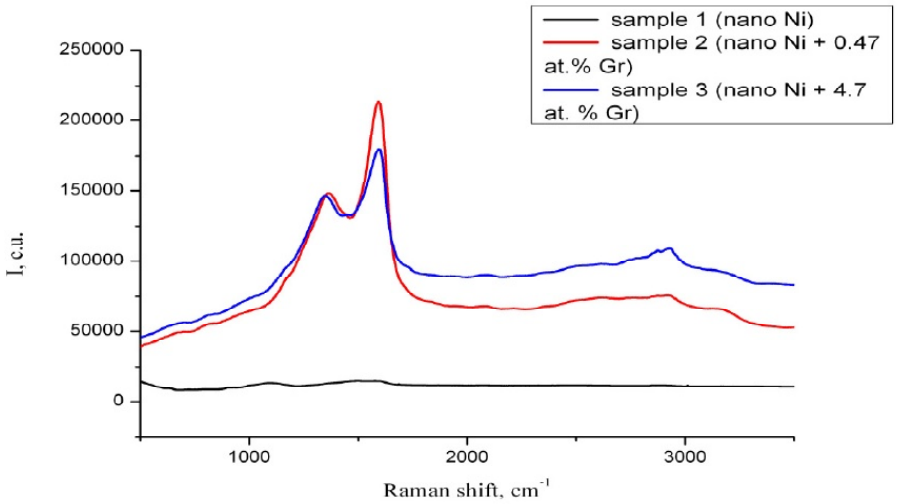

Fig. 6. Raman spectra of Specimens 1, 2, and 3.

DSC results for powders after milling are shown in Fig. 4. As seen from the figure, an exothermic effect attributed to Ni melting is observed for all samples. So, one can conclude that both nickel compounds with graphene-graphite powder (in particular, Ni_3C, see Fig. 1) and solid solution phase are not formed at synthesis temperatures. As solid solution formation often requires more annealing time than it takes place during DSC experiment, the final conclusion on this point was also confirmed by XRD analysis of the annealed specimens (annealing time – 1 hour, cooling in furnace time ~ 6 hrs). Table 1 summarizes the results of thermal analysis, Sample 4 here is the microsized Ni sample provided by NETZSCH as a reference from the standards set.

As seen from the Table, the thermal effects of pure nanosized nickel powder, as well as nanoNi-graphite-graphene composite powders are fairly lower than the effect measured for reference Ni sample (Sample 4). This is likely due to the effect of the excess surface area of the nanoparticles. Some increase in the melting enthalpy with the increase in graphene-graphite content gives an opportunity to assume that such an addition decreases the effect of surface area energy. One can suggest that carbon-containing additions promote nickel grains growth during the thermal analysis procedure; an alternative mechanism could be the formation of sub structure on the nickel particle surface that partially compensates surface energy contribution. XRD patterns of Specimens 1 and 3 fabricated of pure nanosized nickel and composite powder with 4.7 at.% graphite-graphene mixture are shown in Fig. 5a.

One can see that the pure Ni (Specimen 1) is a single-phase material. The composite (Specimen 3) is characterized by a peak in X-ray diffraction pattern at $2\theta=26.5°$, corresponding to pure carbon allotrope(s). At the same time, no peaks corresponding to Ni-carbon compounds or solid solutions are present in the pattern. A detailed examination of the peak at $2\theta=26.5°$ (see a magnified peak in Fig. 5b) demonstrated that it is a superposition of two peaks. Latter indicates the presence of two carbon allotropes – graphene and, likely, graphite in the composite. Further analysis of carbon allotropes was carried out by Raman spectroscopy.

Raman spectra of Specimens 1-3 are demonstrated in Fig. 6. The spectrum of Specimen 1 is typical for metals. Since intensity of G peak at ~1590 nm^{-1} in the spectra of Specimens 2 and 3 is higher than that of 2D peak at 2880 nm^{-1}, one can conclude that few-layer Gr nanoplatelets are present in large amount in composites 2 and 3. Thus, the X-ray diffraction and Raman spectroscopy data (Figs. 5 and 6, respectively) allow us to conclude that carbon in the composites exists in the forms of Gr and graphite, while carbides and carbonyls are absent. The data obtained proves that the most part of graphite to converted into graphene due to mechanical activation during the ball milling.

The intensity of G-peak gives an opportunity to estimate the amount of Gr content in material. It is interesting to note that the intensity of G peak for Specimen 2 with 0.47 at.% of graphite-graphene addition is significantly higher than that for a Specimen 3 with 4.7 at.% of graphite-graphene addition. It means that the amount of graphene in Specimen 2 is higher than in Specimen 3. The key factor of

the tendency observed is, likely, the ratio of surface areas of the composite components: nickel nanopowder and thermally expanded graphite platelets. When the above ratio is optimal, graphene monolayer is preferably formed on the surface of metallic particles. The increase of thermally expanded graphite platelets concentration leads to graphene flakes formation. When the amount of carbon is above some critical value for a given particle size, the formation of the individual graphite phase is possible. The form and intensity of 2D peak at 2880 nm^{-1} corresponds with the ordering of graphene in Specimens 2 and 3. In case of spectra 3, 2D peak is more intensive. The detailed examination of that peak gives a possibility to assume the existence of 7-10 layers in one graphene flake in case of composite 3.

3.2. Samples microstructure

Scanning electron microscopy data on the microstructural observations cleavage surface of specimens 1-3 is shown in Fig. 7. As it follows from Fig. 7a, the structure of Specimen 1 is globular, similar to compact dimpled structure. The incorporation of 0.47 at.% of graphite-graphene phase (see Fig. 7b) results in the structural changes: some part of the surface remains of the same structure (zone I in Fig. 5b), while the most part consists of larger structural elements (zone II in Fig. 5b). One can assume that the enlarged structural elements are the scaled replica of the initial structure of the surface. The presence of 4.7 at.% of graphite-graphene phase leads to major structural changes (see Fig. 7c). The initial structure of pure nickel specimen is almost absent. Compared to zone II in Fig. 7b, the size of structural elements of the surface structure of Specimen 3 even more enlarged. The oval shaped structural elements typical for dimpled structure transformed into polygonal with clearly defined angles and edges (see, zone III in Fig. 7c).

The analysis of microphotos of the specimen surface taken at higher magnification (x10000, Fig. 8) proved the character of structural changes described above. As it is seen from the microphotograph of Specimen 1 (see Fig. 8a), the typical structure elements of pure nanonickel surface are spherical agglomerates with characteristic linear dimensions less than 1 μm. They are likely a result of initial nickel powder agglomeration during specimen's milling and compaction. As it was mentioned before, the average particle size in the initial powder was ~70-80 nm. Even the addition of small amount of graphite-graphene mixture (Specimen 2, Fig. 8b) significantly changes the character of agglomeration processes. Spherical elements are practically absent. Polygonal structures with linear dimensions ~ 1 μm (see elements marked as IV in Fig. 8b) can clearly seen on the background of partially preserved initial structure (zone V, Fig. 8b).

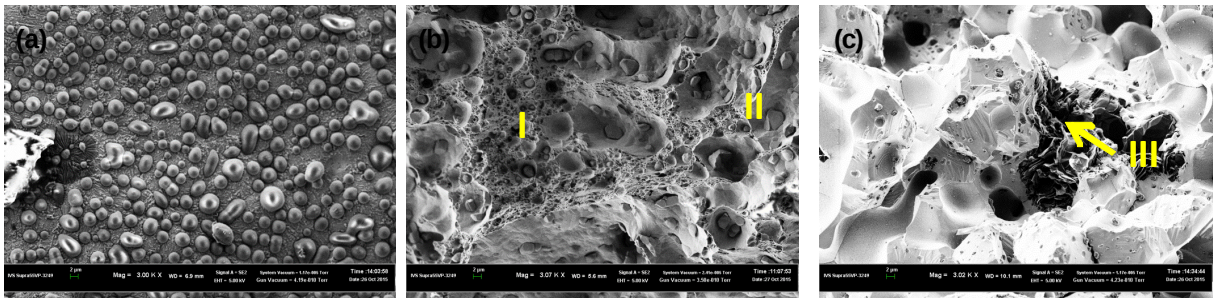

Fig. 7. Evolution of composites structure according to SEM (x3000) data: (a), (b), and (c) – Specimens (1), (2), and (3), respectively.

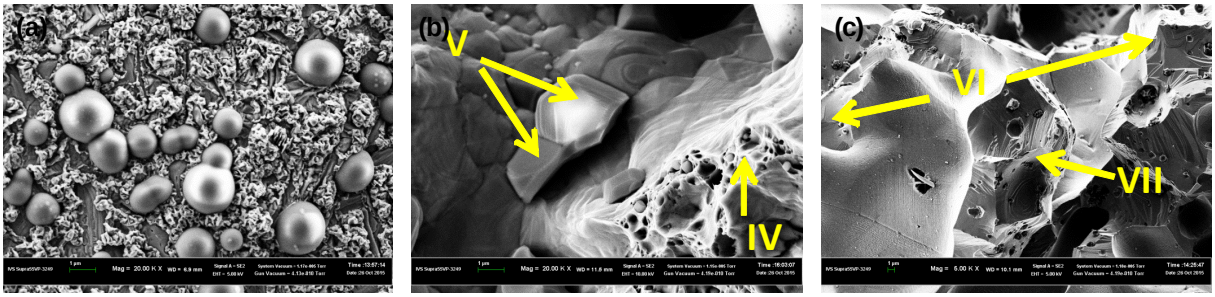

Fig. 8. Evolution of composites structure according to SEM (x20000) data: (a), (b), and (c) – Specimens (1), (2), and (3), respectively.

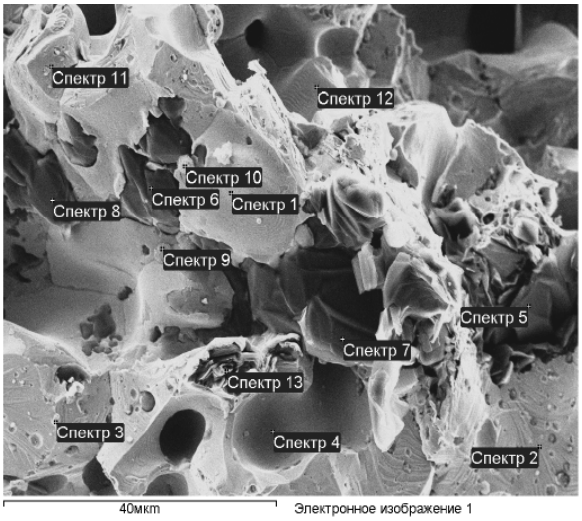

Fig. 9. Microphotograph of Specimen 3 surface with the regions where EDX spectra were obtained.

It should be noted that the liner dimensions of these structures are of the same order of magnitude than the spherical elements observed in Specimen 1. In Specimen 3 with maximal graphite-graphene content (Fig. 8c), linear dimensions of polygonal structural elements significantly increase and can reach up to tenth of micrometers (elements marked as IV in Fig. 8c). The region marked as VII in Fig. 8c is of particular interest as it is most likely a graphene flake, this conclusion is confirmed by chemical analysis of the surface performed by EDX. Table 2 summarizes the results of this analysis, the regions of scanning are shown in Fig. 9.

Interpreting the EDX results presented in Table 2, one should account for the specific experimental features of EDX technique applied here that result in rather high background carbon content in all the spectra is (12-15 wt. %). With regard to this fact, one can state that spectra for regions 1, 2, 11, and 12 correspond to nickel matrix and Ni content can be estimated as being >95 wt.% here. Spectra 5-8 indirectly confirm the presence of graphene flakes. Carbon amount in this regions is >96 wt.%, whereas spectra 4 and 13 are related to “nickel-graphene”. Spectra 9 and 10 give an evidence for the presence of the impurities, that, more likely, were brought in the sample during probe preparation as no one of spectra obtained for Specimens 1 and 2, and the additional measurements undertaken for Specimen 3, did not show such a high amount of oxygen, sulfur, and strontium.

EBSD analysis was performed in order to get the detailed information about the structure of the surface and grain orientation of the composites. Fig. 10 shows the inverse pole figure (IPF) maps of Specimens 1, 2, and 3. It should be noted that the scale bars in Fig. 10 are different for different specimens. Grain size distributions together with grain-boundary character distributions for pure Ni and composite specimens are presented in Fig. 11. Grain size distributions represent the initial information, i.e. the fraction of scanned surface area that is occupied by the grains of certain size. Note that the data for Specimens 1 and 2 was averaged over 3 sites, for Specimen 3 it was averaged over 4 sites. As it is seen from the figure, Specimen 3 (4.7 at.% graphite-graphene mixture) contains grains with linear size 5-35 μm, while in Specimen 1 (pure nickel), the grains with the linear size greater than 5 mm are almost absent. The comparison of Figs. 10 and 11 shows that the main part of grains in the both

Table 2. EDX data on the composition of Specimen 3 (wt.%). The location of the analyzed regions is shown in Fig. 9.

Spectrum	Ni	C	O	Na	Mg	S	Ca	Sr
Spectrum 1	80	19	1					
Spectrum 2	85	14	<1					
Spectrum 4	73	26	2					
Spectrum 5	2	97	<1					
Spectrum 6	3	96	1					
Spectrum 7	1	99	<1					
Spectrum 8	4	95	<1					
Spectrum 9	5	26	18	1	<1	17	19	14
Spectrum 10	3	17	20	1	<1	20	22	16
Spectrum 11	85	14	<1					
Spectrum 12	83	15	2					
Spectrum 13	9	90	<1					

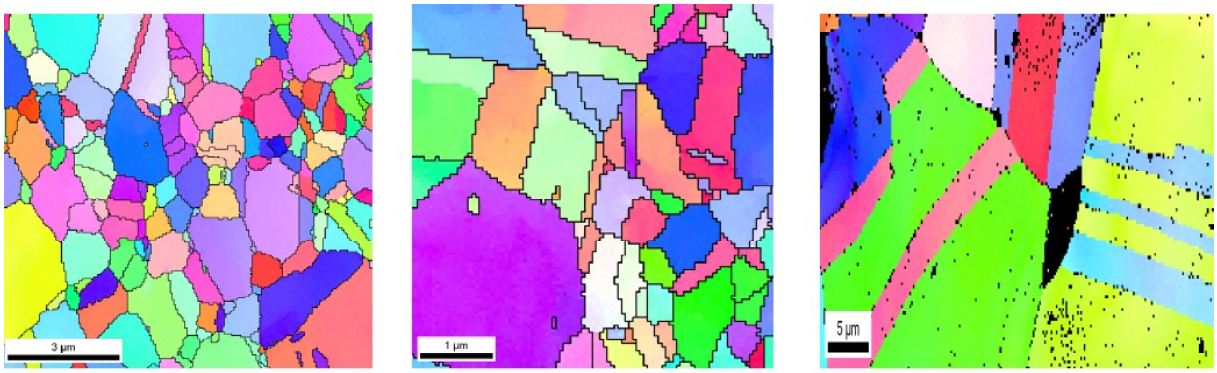

a) b) c)

Fig. 10. Inverse pole figure (IPF) maps of Specimens (a) 1, (b) 2, and (c) 3.

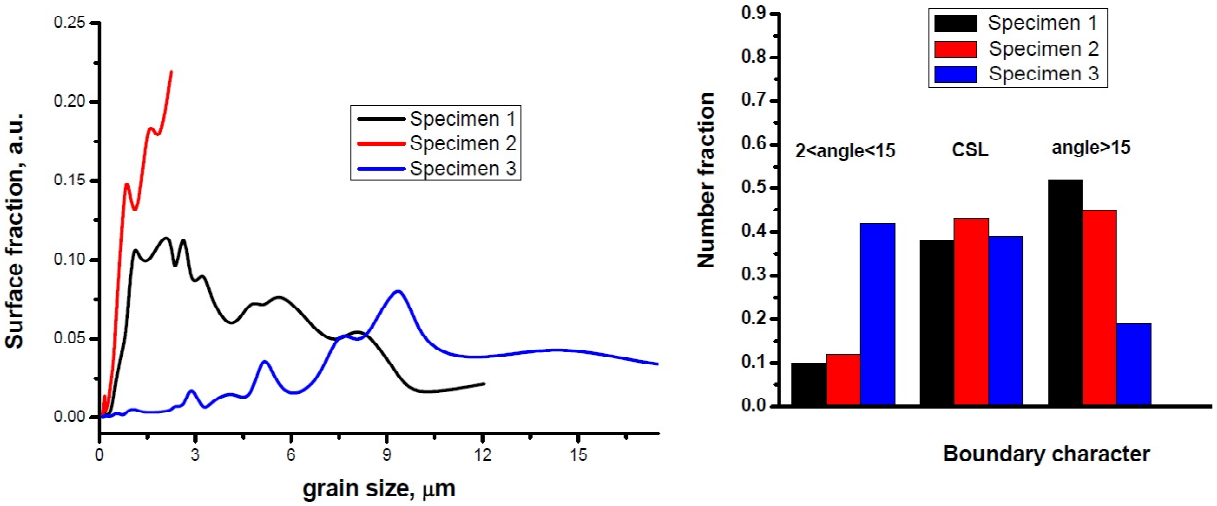

Fig. 11. (a) - grain size distribution (recalculated by number) and (b) grain-boundary character distribution for the specimens under study.

specimens has linear size $d \leq 5$ μm. Pure Ni exhibits grain sizes about 0.25-1.5 μm, while the typical grain size for the composite containing 4.7 at.% of graphite-graphene mixture is about 0.5 μm. It should be mentioned that the data on the grain size determined from EBSD analysis is in the good agreement with linear size of polygonal structures determined by SEM.

In general, the specimens are characterized by bimodal grain size distributions in Ni matrix (Fig. 11, upper row). Specimen 3 is characterized by comparatively high fraction of low-angle grain boundaries (Table 3) and high volume fraction of carbon inclusions (black inclusions in Fig. 10c). These inclusions are treated as graphite that did not transform into Gr during the ball mill treatment. High magnification of the IPF map (Fig. 10c) reveals that graphite inclusions tend to have hexagon-like shape (Fig. 12).

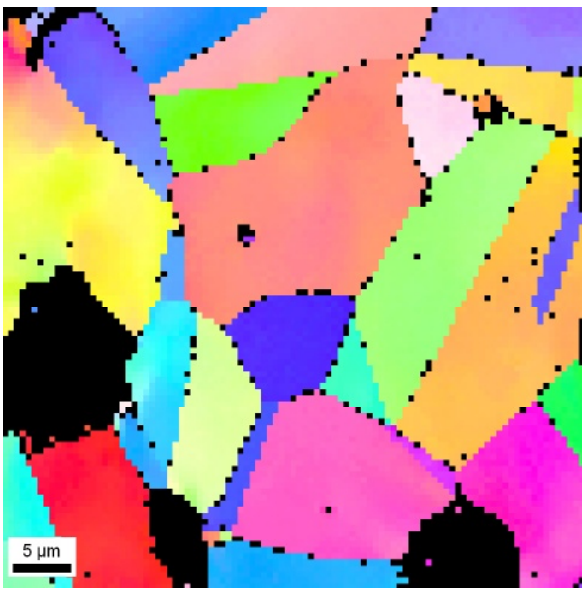

Fig. 12. Magnified IPF map for Ni-4.7 at.% (Gr+graphite) composite. Hexagon-like graphite inclusions are roughly outlined by red hexagons.

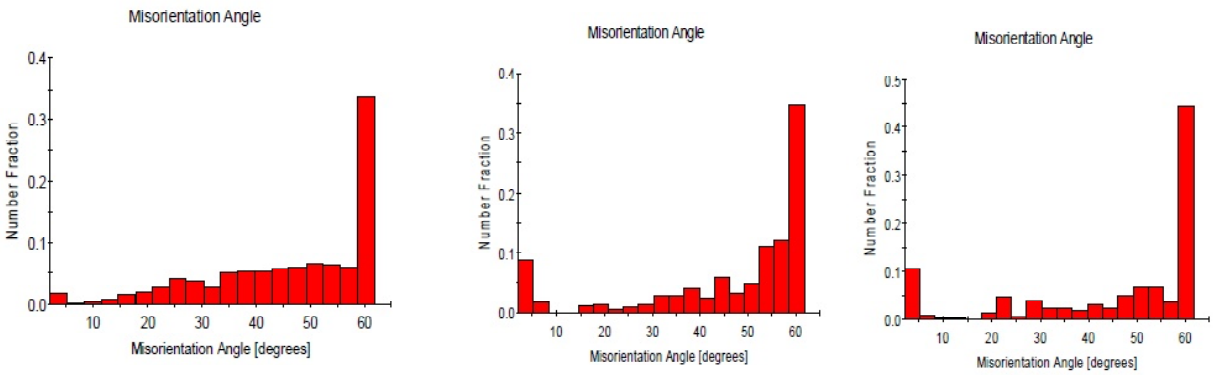

a) b) c)

Fig. 13. Misorientation angle distributions obtained for Specimens (a) 1, (b) 2, and (c) 3.

Misorientation angle distributions obtained for Specimens 1, 2, and 3 are demonstrated in Fig. 13. As seen from the figure, the addition of graphene-graphite mixture results in the increase of low angle misorientations (up to 15°). At the same time, the main fraction of misorientations corresponds to misorientation angles about 60. The data obtained on that fraction increase from 35 and 37 to 45% for Specimens 1, 2, and 3, respectively, can be explained in terms of graphene-graphite mixture increase. However that tendency requires the additional experimental tests.

3.3. Mechanical characteristics

Mechanical properties of pure nickel (Specimen 1) and composites 2 and 3 in the compression mode were estimated by three parameters which describe the main features of their mechanical behavior, such as compression yield limit ($\sigma_{0.2}$), ultimate stress (σ_T), and plastic strain value (ε). The results of the tests are presented in Fig. 14. As it is seen from the stress-strain diagram, pure nanonickel exhibits brittle and ductile deformation type. The deformation of globular structure takes place without strengthening indicating high closed porosity of the specimen. The process is likely accompanied by pore walls collapse. Latter causes the change in the area of force application. That could also contribute in the observed deformation character. The hypothesis is confirmed by fractography data (see Fig. 15a). In particular, pure Ni and Ni-0.47 at.% (Gr+graphite) specimens exhibit moderate values (~ 235 and ~ 410 MPa, respectively) of the compressive stress, while strain-to-failure ε_f ~ 7% of pure Ni is larger than ε_f ~ 1% of and Ni-4.7 at.% (Gr+graphite) composite.

The addition of graphene-graphite mixture results in the changes in deformation character to more

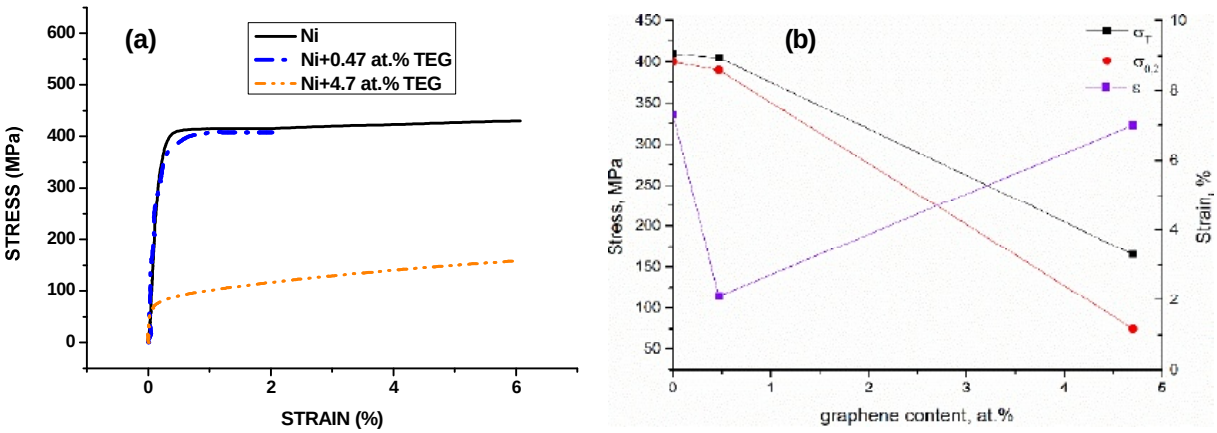

Fig. 14. The data on mechanical testing of the samples (a) Stress-strain dependencies for Specimens 1, 2, and 3 in compression test; (b) the dependencies of $\sigma_{0.2,}$ σ_T, and ε on graphene content.

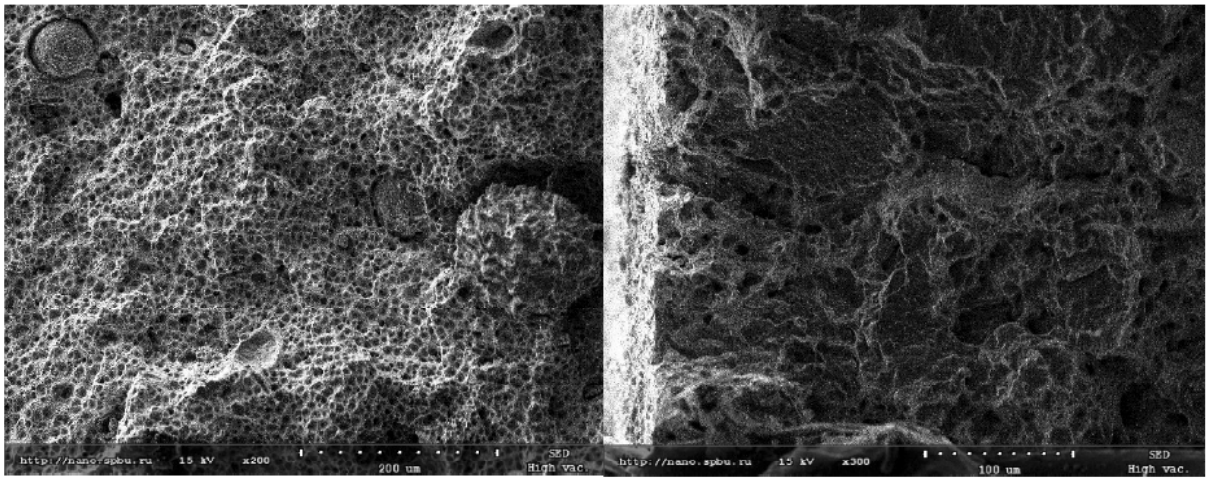

Fig. 15. The results of phactography of (a) Specimen 1 and (b) Specimen 2.

brittle for Specimen 2 (0.47 at.% graphite-graphene mixture) and ductile for Specimen 3 (4.7 at.% graphite-graphene mixture). The incorporation of small amount of graphite-graphene mixture leads to ductility suppression without strength value change. However, further increase of graphite-graphene mixture content leads to ductility recover accompanied with strength decrease. The comparison of SEM and mechanical tests data allows to assume that the change in deformation character can be related to the transformation of globular microstructure to polygonal, characterized by large structural elements size and low closed porosity up on graphite-graphene mixture content increase. Strain-to-failure $\varepsilon_f \sim 7\%$ of Ni – 4.7 at.% (Gr+graphite) composite is by practice the same as with pure Ni (Fig. 14). However, flow stresses characterizing the former material are much lower than those specifying pure Ni (Fig. 14). The low flow stress of Ni-4.7 at.% (Gr+graphite) composite can be related to its larger grain size (see Fig. 11 upper row), as compared to those in counterpart Specimens 1 and 2 as because strength of metals typically decreases with rising grain sizes.

The assumption on deformation mechanism in the composite is confirmed by Vickers hardness data obtained. Vickers hardness dependence on graphite-graphene mixture content is shown in Fig. 16. As seen from the figure, the dependence of Vickers hardness on graphite-graphene content has a maximum. The incorporation of 0.47 at.% graphite-graphene mixture to Ni matrix results in insignificant hardness increase, further increase of dopant content leads to hardness decrease.

4. CONCLUSIONS

It was shown that the addition of 0.47 at.% graphite-graphene mixture results in ductility decrease with no decrease in the initial strength, and slight Vickers hardness increase of graphene-modified bulk nuickel composites. Using XRD and Raman spectroscopy methods it was confirmed that up on the small addition of graphite-graphene mixture the most part of graphite converts to graphene flakes having 5-7 graphene layers; graphene flakes are distributed on the surface of metal particles. It was revealed, that Gr flakes in bulk nickel 0.47 at.% graphene reinforced composites composite eliminate grain growth during its synthesis so that this composite has a comparatively small grain. Ni-4.7 at.% Gr+graphite composite is characterized by

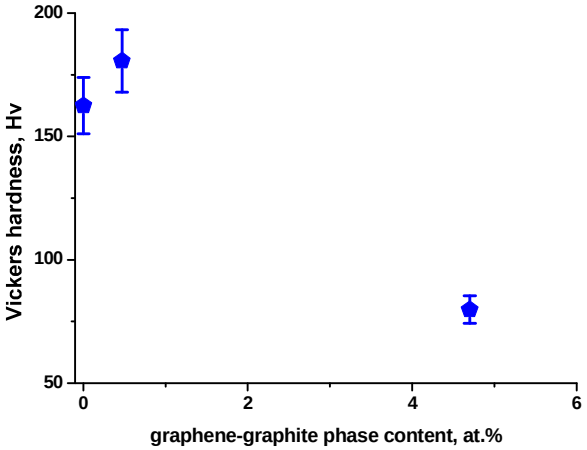

Fig. 16. Vickers hardness dependence on graphite-graphene mixture content.

comparatively large mean grain size (~6 μm) and high volume fraction of graphite inclusions. Bimodal grain size distributions have been observed in the composite samples. The stress-strain dependences showed no enhancement of strength and ductility in bulk nickel due to Gr reinforcement.

ACKNOWLEDGEMENTS

This work was supported by the Russian Science Foundation (project 14-29-00199). Raman spectroscopy reseach was performed at the Center for Optical and Laser Materials Research at Research park in St. Petersburg State University. Differential scanning calorimetry were performed at the Research park of St. Petersburg State University Center for Thermogravimetric and Calorimetric Research.

REFENENCES

[1] K.S. Novoselov, A.K. Geim, S.V. Morozov, D. Jiang, Y. Zhang, S.V. Dubonos and A.A. Firsov // *Science* **306** (2004) 666.

[2] A.K. Geim and K.S. Novoselov // *Nature Materials* **6** (2007) 183.

[3] N. Levy, S.A. Burke, K.L. Meaker, M. Panlasigui, A. Zettl, F. Guinea, A.H. Castro Neto and M.F. Crommie // *Science* **329** (2010) 544.

[4] L.L. Zhang, R. Zhou and X.S. Zhao // *Journal of Materials Chemistry* **20** (2010) 5983.

[5] H.J. Yoon, D.H. Jun, J.H. Yang, Z. Zhou and M.M. Cheng // *Sensor and Actuators B* **157** (2011) 310.

[6] M.C. Chung, D.H. Kim, H.M. Lee, T. Kim, J.H. Choi, D.K. Seo, J. Yoo, S. Hong, T.J. Kang and Y.H. Kim // *Sensor and Actuators B* **166-167** (2012) 172.

[7] F. Xia, D.B. Farmer, Y.M. Lin and P. Avouris // *NanoLetters* **10** (2010) 715.

[8] J-L. Tsai and J-F. Tu// *Mater Des* **31** (2010) 194.

[9] C. Lee, X. Wei, J.W. Kysar and J. Hone // *Science* **321** (2008) 385.

[10] C. Lee, X. Wei, Q. Li, R. Carpick, J.W. Kysar and J. Hone // *Phys Status Solidi (B)* **246** (2009) 2562.

[11] T. Kuilla, S. Bhadra, D. Yao, N.H. Kim, S. Bose and J.H. // *Progress in Polymer Science* **35** (2010) 1350.

[12] M.A. Rafiee, J. Rafiee, Z. Wang, H. Song, Z-Z. Yu and N. Koratkar // *ACSNano* **12** (2009) 3884.

[13] M.A. Rafiee, J. Rafiee, Z-Z. Yu and N. Koratkar // *Applied Physics Letters* **95** (2009) 131.

[14] S.C. Tjong // *Mat. Sci. and Eng R* **74** (2013) 281.

[15] I. Firkowska, A. Boden, A.M. Vogt and S. Reich // *J. Mater. Chem.* **21** (2011) 1754.

[16] J. Wang, Z. Li, G. Fan, H. Pan, Z. Chen and D. Zhang // *Scr. Mater.* **66** (2012) 594.

[17] L.Y. Chen, H. Konishi, A. Fehrenbacher, C. Ma, J.Q. Xu, H.S. Choi, H.F. Xu, F.E. Pfefferkorn and X.C. Li // *Scr. Mater*. **67** (2012) 29.

[18] C.L. Pavithra, B.V. Sarada, K.V. Rajulapati, T.N. Rao and G. Sundararajan // *Scientific Reports* **4** (2014).

[19] J.A. Hooker and P.J. Doorbar // *Materials science and technology* **16** (2000) 725.

[20] D.B. Miracle // *Composites science and technology* **65** (2005) 2526.

[21] J.W. Kaczmar, K. Pietrzak and W. Wlosinski // *Journal of materials processing technology* **106** (2000) 58.

[22] W. B. Eisen, In: *Proceeding ofI nternational Techno-Business Conference on the Superalloys Industry" Superalloys for Gas Turbine"* (Tampa, Florida, USA), p. 4.

[23] H. Gui, F. Kilic, M.Uysal, S.Aslan, A. Alp and H. Akbulut // *Applied Surface Science* **258** (2012) 4260.

[24] P.W. Leech, X.S. Li and N. Alam // *Wear* **294-295** (2012) 380.

[25] H. Gui, F. Kilic, M.Uysal, S.Aslan, A. Alp and H. Akbulut // *Wear* **267** (2009) 976.

[26] J.Y. Hwang, B.K. Lim, J. Tiley, R. Banerjee and S.H. Hong // *Carbon* **57** (2013) 282.

[27] C. Zhao // *Applied Physics A* **118** (2015) 409

[28] S.M. Uddin, T. Mahmud, C. Wolf, C. Glanz, I. Kolaric, C. Volkmer, H.Höller, U.Wienecke, S.Rothand and H-J.Fecht // *Composites Science and Technology* **70** (2010) 253.

[29] V. Rajkovic, D. Bosic and M.T. Jovanovich // *Materials and Design* **31** (2010) 1962.

[30] M. Khakbiz and F. Akhalghi // *Journal of Alloys and Compounds* **479** (2009) 334.

[31] H. Abbaszadeh, A. Masoudi, H. Safabinesh and M. Takestani // *Int. Journal of Refractory Metals and Hard Materials* **30** (2012) 145.

[32] O. Kurapova, E.N. Solovieva, I.V. Lomakin, S.N. Sergeev, N.N. Novik, I.Yu. Archakov, A.P. Zhilyaev, V. G. Konakov // *Composites part B: Engineering* , submitted.

[33] L. Kvetkova, A. Duszova, P. Hvizdoš, P. Kun and C. Balázsi // *Scripta Materialia* **66** (2012) 793.
[34] V.G. Konakov, I.A. Ovid'ko, N.V. Borisova, E.N. Solovyeva, S.N.Golubev, O.Yu Kurapova, N.N. Novik and I.Yu. Archakov // *Reviews on advanced material science* **39** (2014) 41.
[35] V.N. Danilenko, S.Yu. Mironov, A.N. Belyakov and A.P. Zhilyaev // F*actory laboratory. The diagnostics of materials* **78** (2012) 28, In Russian.
[36] P. Gustafson, A. Gabriel and I. Ansara // *Z. Metallkd.* **78** (1987) 151.
[37] D. T. Hawkins and R. Hultgren, In: Metals Handbook, Vol. 8., ed. by L. Taylor (American Society of Metals, Metals Park, Ohio, 1973), p. 251.